Article

Polymer Waveguide Sensor Based on Evanescent Bragg Grating for Lab-on-a-Chip Applications

Zhenyu Zhang *, Ahmad Abdalwareth, Günter Flachenecker, Martin Angelmahr, Wolfgang Schade

Posted Date: 19 December 2023

doi: 10.20944/preprints202312.1340.v1

Keywords: optical sensor; Bragg grating; polymer waveguide; lab-on-a-chip; on-chip optical sensor; evanescent field sensor; nanoparticles; hydrogen sensor

Article

Polymer Waveguide Sensor Based on Evanescent Bragg Grating for Lab-on-a-Chip Applications

Zhenyu Zhang [1,2,*], Ahmad Abdalwareth [1,2], Günter Flachenecker [1], Martin Angelmahr [1] and Wolfgang Schade [1,2]

[1] Department for Fiber Optical Sensor Systems, Fraunhofer Heinrich Hertz Institute, 38640 Goslar, Germany
[2] Institute of Energy Research and Physical Technologies, Clausthal University of Technology, 38640 Goslar, Germany
* Correspondence: zhenyu.zhang@hhi.fraunhofer.de

Abstract: In this work, an evanescent Bragg grating sensor inscribed in a few-mode planar polymer waveguide was integrated in microchannel structures and characterized with various chemical applications. The planar waveguide and the microchannels consisted of epoxide-based polymers. The Bragg grating structure was post-processed using point-by-point direct inscription technology. By monitoring the central wavelength shift of the reflected Bragg signal, the sensor showed a temperature sensitivity of -47.75 pm/K. Moreover, the functionality of the evanescent field-based measurements is demonstrated with two application examples: refractive index sensing of different aqueous solutions and gas-phase hydrogen concentration detection. For the latter application, the sensor was additionally coated with a functional layer based on palladium nanoparticles. During the refractive index sensing measurement, the sensor achieved a sensitivity of 6.5 nm/RIU from air to 99.9% pure isopropyl alcohol. For the gas-phase hydrogen detection, the coated sensor achieved a reproducible concentration detection up to 4 vol% hydrogen. According to the reported experimental results, the integrated Bragg grating-based waveguide sensor demonstrates high potential for applications based on lab-on-a-chip concept.

Keywords: optical sensor; Bragg grating; polymer waveguide; lab-on-a-chip; on-chip optical sensor; evanescent field sensor; nanoparticles; hydrogen sensor

1. Introduction

Devices based on lab-on-a-chip (LOC) technology offer a variety of miniaturized fluidic and non-fluidic systems for chemical and biological applications [1]. LOC devices possess the advantages of miniaturized size, fast response with small volumes samples and low cost analysis [2]. During the past few decades, the potential of LOC devices have been widely explored with various micro-engineered sensor platforms embedded in the device that allows various chemical or biological measurements [3]. In this case, optical sensors, especially Bragg grating-based sensors, due to their small size and low power requirements for operation, have driven increasingly attention to be integrated as a sensor element in LOC devices [4,5].

Bragg gratings are periodic spatial modulations of the refractive index along the optical waveguide. One of the most common Bragg grating sensors are fiber Bragg gratings (FBGs) inscribed with laser inside silica-based fiber core [6]. Since first introduced by Kawasaki et al. in 1978 [7], FBGs have been widely investigated for indirect measurements in physical and chemical areas [8]. However, the protective sheath of the conventional fibers limits the direct interaction of the guided optical mode with the surrounding medium. To enable evanescent interaction with the FBG sensors, a chemical etching process is often required to remove the cladding of the silica fiber. The resulted etched fiber Bragg grating (eFBG) sensor can be directly applied for measuring various refractive indices from different liquid solutions [9], moreover, a LOC device integrated with an eFBG sensor has been presented by Lee et al. for measuring microstrain, temperature and refractive indices [10].

 doi:10.20944/preprints202312.1340.v1

Nevertheless, optimizations can still be made to further increase the stability and sensitivity of the integrated Bragg grating sensor in both fabrication and measurement processes. For instance, through the etching process, the eFBG signal may shift from the original addressed Bragg wavelength and intensity, in extreme cases, alter the original signal completely [11]. These possible variations during the etching process typically results in a lowered reproducibility of the eFBG sensors. Furthermore, since polymer is one of the commonly used materials for LOC devices, eFBGs cannot be embedded in LOC devices consist of polymer materials that possesses a greater refractive index than the fiber core; otherwise, the light transmitted through the fiber core will be completely coupled into the surrounding polymers, resulting in loss of the signal. To overcome these disadvantages, polymer planar optical waveguides could be a better alternative replacing etched silica-based fiber for LOC device integration. For example, Meyer et al. presented a polymer waveguide inscribed with Bragg grating structures, the sensor showed an increased sensitivity compared to FBGs in temperature and strain respectively [12]. However, their presented polymer waveguide Bragg grating sensor was not directly applicable for evanescent field detection, as they used a polymer cladding, shielding the waveguide from the surrounding media. A polymer waveguide without cladding would enable the evanescent wave interaction and opens more applications like refractive index sensing and more precise chemical detection capabilities coated with functional layers.

Functional layers are commonly used for optical sensors to achieve a selective detection of specific gases [13,14]. This possibility makes optical sensors attractive as general sensor platforms, which can be functionalized individually, depending on the target molecules to be detected. For example, Kefer et al. presented a laser infused evanescent polymer waveguide Bragg grating sensor coated with Pt-loaded $WO_3 - SiO_2$ which achieved achieved a detection limit of 5 ppm hydrogen in air [15]. This methodology provides a possibility for optical hydrogen sensors implementable in LOC devices and provides great potential for researches investigating underground bio-methanation reactor concept, in which hydrogen and carbon dioxide are converted into methane inside underground porous formations. This concept has been attracting increasingly attention under the high demanding hydrogen energy research in recent years [16]. However, a wider sensor dynamic range than ppm area for hydrogen detection is desirable for specific applications like analyzing efficiency of the methanation reaction [17]. In this case, most recently, Abdalwareth et al. presented an eFBG sensor coated with palladium nanoparticles and achieved a hydrogen detection up to 5 vol% [18]. It is most interesting to investigate if the same coating can be applied on a planar polymer waveguide sensor based on Bragg grating structures.

In this work, we present an evanescent Bragg grating sensor based on polymer waveguide, which was manufactured simultaneously alongside the LOC structure using same processing steps. The air-cladded few-mode ridge waveguide consisted of epoxide-based polymers. The waveguide was patterned with photo resist epoxy applied on a silica glass substrate using photolithography technology. The Bragg grating structure was inscribed subsequently into the waveguide by a femtosecond laser within a separate processing step. The temperature dependence of the ridge waveguide Bragg grating (RWBG) sensor was characterized for different ambient temperatures from 20 °C to 60 °C. Further, the performance of the sensor for detection of chemicals was validated and demonstrated by both, liquid-phase refractive index measurement with different concentrated isopropyl alcohol (IPA) solutions as well as gas-phase hydrogen detection. For hydrogen detection, the sensor was additionally coated with palladium nanoparticles.

2. Materials and Methods

2.1. Waveguide Fabrication

The fabrication process begins with an oxygen plasma treatment for the glass substrate to create a hydrophilic surface for the optimal adhesion. After the oxygen treatment, a substrate layer for the waveguide, consisting of EpoClad2 from micro resist technology GmbH is deposited on the oxygen

Preprints (www.preprints.org) | NOT PEER-REVIEWED | Posted: 19 December 2023 doi:10.20944/preprints202312.1340.v1

activated surface of the substrate with a spin-coating process. The substrate polymer has a refractive index of 1.57 at 830 nm, which is lower than the polymer EpoCore5 (refractive index 1.58 at 830 nm) used for patterning the waveguide [19]. The substrate layer aims to ensure the optical confinement of the guided light in the waveguide that is applied on top of this substrate layer. The layer thickness of the polymers depends on the spin-coater speed, here the substrate polymer is adjusted to 2 µm. After the spin-coating process, the glass substrate with the EpoClad2 layer was pre-baked for 5 min at 120 °C. Subsequently, after applying flood exposure with UV light, the polymer substrate was hard-baked on a heat plate with 120 °C for 30 min. After the polymer substrate was prepared, its surface was again activated with oxygen plasma. Immediately after this, we added a 5 µm layer of Epocore5 on top of it via spin coating. The substrate with both layers was then pre-baked on a heat plate with subsequently 50 °C for 2 min and 90 °C for 4 min. Afterwards, we applied a waveguide pattern by using a UV-photolithography machine (µPG 101, Heidelberg instruments). Consequently, the substrate with patterned polymers was post-baked on the heat plate with the same parameters from pre-bake processes. Finally, the substrate with polymer layers was immersed in the developer (mrDev600, micro resist GmbH) for 3 min to resin the remaining unexposed polymers. A final hard-bake process on the heat plate with 120 °C for 30 min concluded the fabrication process for the ridge waveguide and thus, the waveguide is then ready for Bragg grating inscription. The waveguide enlarged with a 100× objective and its cross-section profile measured with a laser scanning microscope (LSM) (VK-X250, Keyence Deutschland GmbH) is displayed in Figure 1(c), the cross-section profile of the waveguide shows a dimension of 6.5 µm width and 5 µm height.

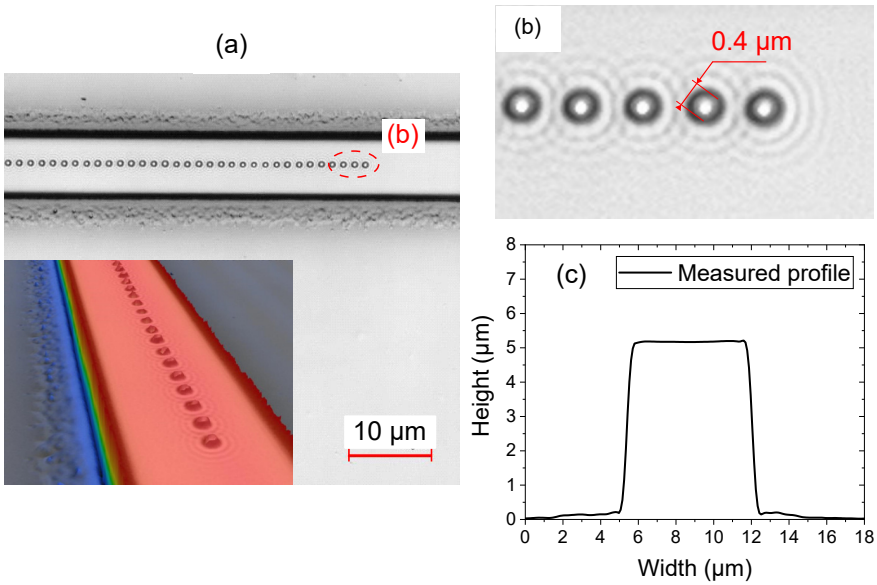

Figure 1. (**a**) Microscopic photo of the RWBG (inlet: 3D height profile). (**b**) An enlarged area demonstrating the laser-inscribed Bragg grating structure. (**c**) Cross-section profile of the polymer ridge waveguide.

2.2. Bragg Grating Inscription

We applied femtosecond laser pulses to achieve uniform periodic refractive index modulations along the polymer waveguide. Such Bragg grating structures are spectral small band mirrors with a central reflection wavelength λ_B [6]:

$$\lambda_B = \frac{2n_{eff}\Lambda}{m}, \tag{1}$$

where n_{eff} is the effective refractive index, Λ represents the grating period and m is the grating order determined as a natural number. For a central wavelength $\lambda_B = 850\,nm$, the period of the grating points Λ is calculated to be 1.43 µm for the 5th grating order.

Preprints (www.preprints.org) | NOT PEER-REVIEWED | Posted: 19 December 2023 doi:10.20944/preprints202312.1340.v1

The setup for Bragg grating inscription consists of a commercially available femtosecond laser (Ti/sapphire Tsunami/Spitfire pro, Spectra-Physics). The laser pulses had a central wavelength of 800 nm and the pulse duration was 85 fs [20]. The substrate with the ridge waveguide was fixed on three translation stages (N-565.260, N-565.360 and E-709, Physik Instrumente) for enabling high-precision three-dimensional movements during the Bragg grating inscription process. During this process, the laser pulses were focused by a 20× objective lens (LD Plan-Neoflur 20×, Carl Zeiss AG), the energy of the laser was set at 29 nJ at a repetition of 10 Hz measured under objective lens. A detailed picture of the Bragg grating taken by LSM is displayed in Figure 1(a). The inlet picture in Figure 1(a) shows a three-dimensional profile of the waveguide including the laser inscribed Bragg grating structure, measured by LSM. Figure 1(b) shows a top view of the refractive index modulation points caused by single laser pulses, the average radius of the grating points was 0.4 µm.

2.3. Sensor Integration in LOC Concept

In this work, we designed a T-junction microchannel structure to guide test fluids onto the sensor position, the overall size of the microchannel structure is 30 mm in square, its sketch is displayed in Figure 2(a). The designed structure consists of one broader microchannel that holds the waveguide and two narrower microchannels enabling the external injection of liquids into the main channel. On the tips of all three microchannels are inlet positions that allow the connection of external fluid injection or can be used as waste outlet. In this concept, the RWBG will serve as an optical sensor element, enabling in-situ measurement of refractive indices from liquid solutions.

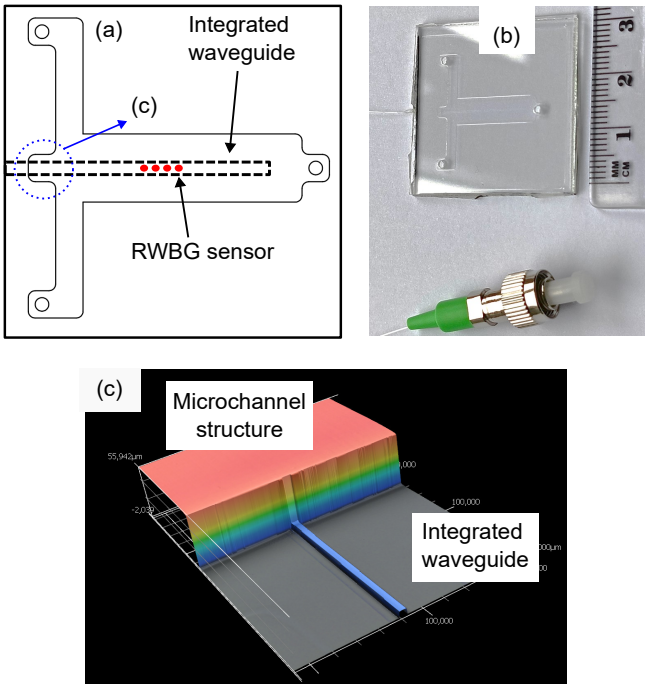

Figure 2. T-junction structure for LOC sensor integration: (**a**) Sketch of the T-junction design and positioning of the waveguide and RWBG. (**b**) A photo of the RWBG sensor chip. (**c**) A 3D height profile where the 5 µm high waveguide channels through a 50 µm high microstructure.

The fabrication of the T-junction structure took place directly after the Bragg grating inscription. It began with the application of an additional polymer resist layer of EpoClad50 (with 50 µm layer thickness) onto the RWBG sensor surface. After the polymer deposition was finished using spin-coater, the T-junction structure was patterned by the same photolithography machine (see section 2.1). In Figure 2(c), a 3D laser scanning height profile of the place is shown, where the ridge waveguide tunnels through the higher microchannel boundary.

Preprints (www.preprints.org) | NOT PEER-REVIEWED | Posted: 19 December 2023 doi:10.20944/preprints202312.1340.v1

Lastly, the sealing of the T-junction structure took place by adhering another polymer-applied glass substrate as the top seal of the microchannels, forming a compact LOC device. The sealing glass substrate includes boreholes on positions where the corresponding inlet channels from the T-junction structure are located. Another EpoClad50 layer with a layer thickness of 50 µm was applied on the surface of the sealing glass substrate to serve as bonding polymer to adhere to the microchannel layer. Afterward, the two substrates were pressed together, followed by a hard-bake process, completing the fabrication for a RWBG integrated compact LOC device. The fabricated LOC device is displayed in Figure 2(b). The optical read-out of the RWBG was realized by butt-coupling a single-mode glass fiber to one open end of the waveguide at the edge of the LOC sensor chip using a 3-axis positioning stage (MAX313D/M, Thorlabs, Inc.) and fixed onto the end of the waveguide with UV adhesive (PO-67-LS, Dymax Europe GmbH).

2.4. Functional Coating for Hydrogen Detection

Aside from being used as an evanescent sensor in liquid-phase refractive index measurement, the RWBG sensor is also capable of selective sensing of gases by applying a functional coating. Here, we demonstrate this functionality concept by using palladium nanoparticles as the functional coating for selective hydrogen gas detection. For preparation of the coating process, we exposed the surface of the RWBG sensor with oxygen plasma to ensure a hydrophilic surface. Then we wetted the sensor with drops of a dissolved palladium nanoparticles solution until the whole grating area was fully covered. The palladium nanoparticles (HiQ-Nano s.r.l., Italy) used here possess an average size of 8 nm and a size distribution between 7 nm and 9 nm; the nanoparticles were dissolved in distilled water with a concentration of 1 mg/mL. This coating process was monitored in real-time with the optical measurement setup presented in Figure 3. Finally the intensity of the RWBG reflection signal decreased up to the half of the original position. In the meantime, the palladium nanoparticle solution on the sensor surface was visually vaporized.

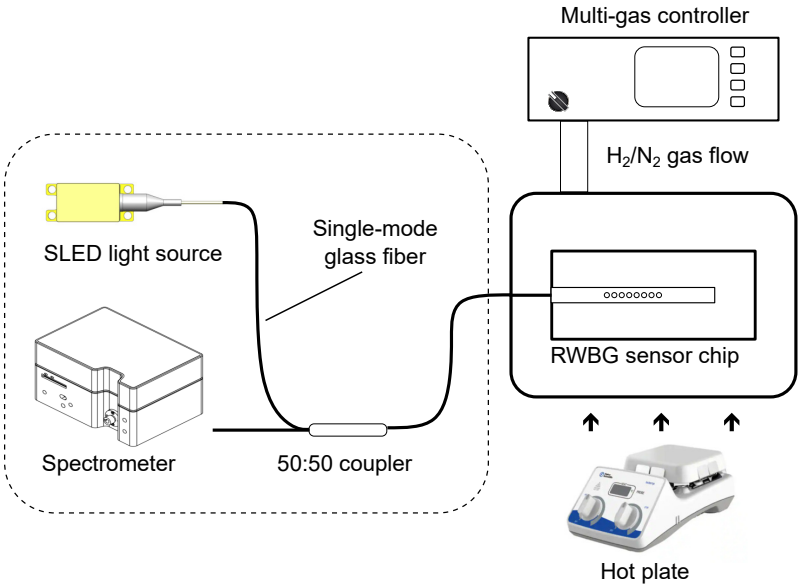

Figure 3. Optical measurement setup and read-out unit.

2.5. Optical Measurement Setup

To evaluate the read-out signal of the RWBG, a broadband SLED with a center wavelength of 840 nm (EXS210006-01, EXALOS AG) was used as light source, the emitted light beam was coupled through a 50:50 fiber coupler and transmitted into the RWBG and finally, the back reflected Bragg signal was coupled via the fiber coupler into a spectrometer (Flame-S-VIS-NIR, Ocean Insight). The optical measurement setup is illustrated in Figure 3 inside the dashed line area. As the RWBG sensor

Preprints (www.preprints.org) | NOT PEER-REVIEWED | Posted: 19 December 2023 doi:10.20944/preprints202312.1340.v1

chip was connected only via a single glass fiber to the interrogator, the flexibility of handling the chip to different experimental setups was high. To test the sensor at different temperature conditions, the RWBG sensor chip was placed on a tunable hot plate (Fisherbrand Isotemp, Fisher Scientific GmbH).

For the gas-phase hydrogen measurement, the sensor chip was enclosed in an experimental gas chamber with a connection to gas flow controller system (647C, MKS Instruments GmbH, Germany) to adjust different concentrations of gas mixtures.

3. Results

3.1. RWBG Reflection Spectrum and Temperature Dependence

The reflection spectrum of the RWBG, achieved with the fiber-coupled measurement setup shown in Figure 3, is displayed in Figure 4(a).

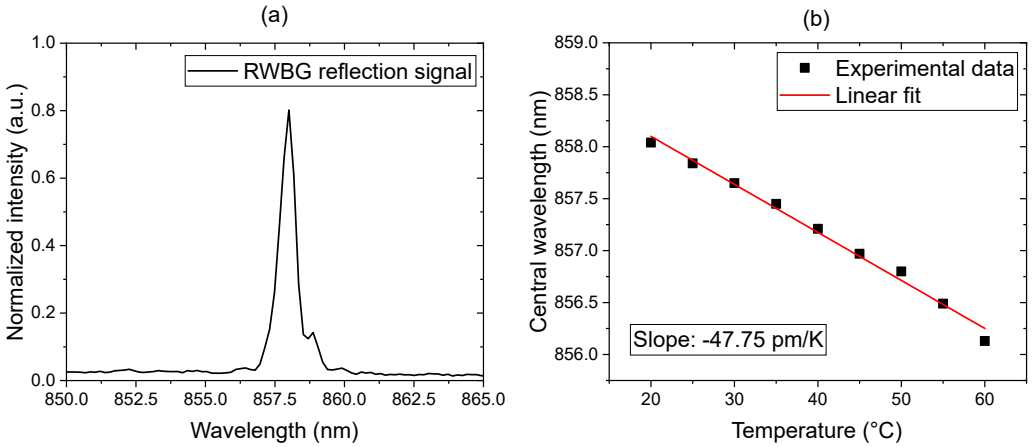

Figure 4. (**a**) Reflection spectrum of the RWBG. (**b**) Temperature dependence measurement result.

To evaluate the temperature sensitivity of RWBG, the sensor chip was placed on a hot plate. We started the measurement at room temperature (20 °C with 40% humidity level). Subsequently, the temperature of the hot plate was increased stepwise of 5 °C until a temperature of 60 °C was reached. During the experiment, the central wavelength of the reflected Bragg signal was monitored continuously at each temperature level. The measurement results are shown in Figure 4(b). As can be seen from these measurement data, the wavelength of the Bragg reflection is decreasing linearly with a slope of -47.75 pm/K with increasing temperature. The temperature sensitivity of the sensor is similar to the waveguide Bragg grating sensor presented by Meyer et al., who used the same photo resist for the fabrication of their non-evanescent sensors and achieved -44 pm/K temperature sensitivity under 42.5% humidity level [12]. Compared to an integrated eFBG sensor based on silica fiber from Lee et al., which achieved a temperature sensitivity of -13 pm/K, our RWBG sensor shows a 3.7× higher temperature sensitivity performance [10]. On the other hand, comparing to the FBG sensor inscribed in a polymer optical fiber presented by Pospori et al., which demonstrated a temperature sensitivity of 21.5 pm/K for increasing temperature measurement without pre-strain, our presented RWBG sensor also shows a 2.2× better performance in temperature sensing [21].

3.2. Liquid-phase Evanescent Field Measurement: Refractive Index Sensitivity

To validate the functionality of direct liquid-phase evanescent field measurement, aqueous IPA solutions with different concentrations, ranging from 0-99.9%, were successively applied on the RWBG sensor integrated in the LOC device guided by the T-junction microchannel structure. Within the experiment, the aqueous IPA solutions were manually injected into the RWBG sensor chip through one inlet channel with a syringe until the Bragg grating was immersed completely with the test solution. At the same time, the central wavelength shift of the reflection signal was monitored with the optical

Preprints (www.preprints.org) | NOT PEER-REVIEWED | Posted: 19 December 2023 doi:10.20944/preprints202312.1340.v1

measurement setup introduced in Figure 3. When the signal stabilization was reached, the liquid was pressed out with air injection, so that the monitored Bragg wavelength could return to the original position. The result of this measurement is displayed in Figure 5(a).

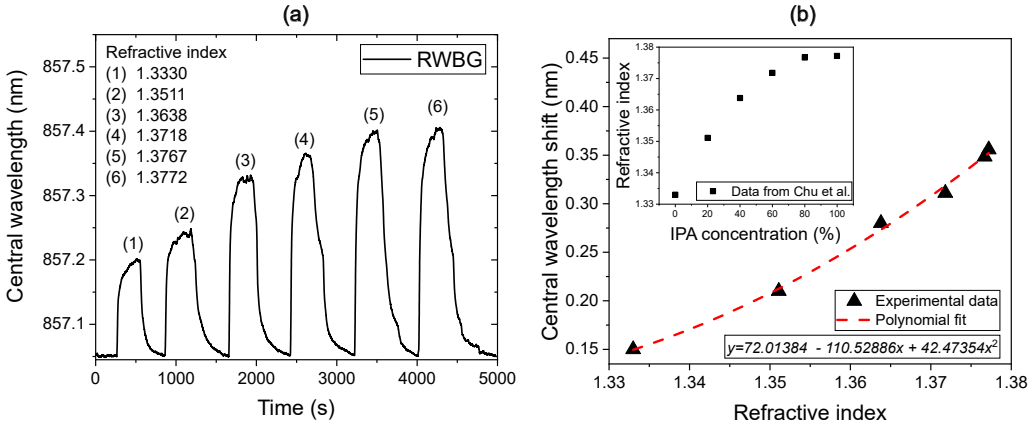

Figure 5. (**a**) Monitored RWBG central wavelength shift course when flushed with aqueous solutions with different IPA concentrations. (**b**) Plotted measurement points fitted with a polynomial function, the adopted refractive indices are displayed in the inlet.

During the measurement, the monitored shift of the RWBG central wavelength increased noticeably, when the sensor surface was wetted with IPA solutions, the average sensor response time lies at 120 s. The RWBG central wavelength shifts depending on the refractive indexes of the different surrounding aqueous IPA solutions are displayed in Figure 5(b), here we adopted the refractive index of the corresponding IPA solutions from Chu et al. [22], which are additionally shown in the inlet of Figure 5(b). The overall sensor response during the measurement can be fitted with a polynomial function.

According to the data in Fig 5(b), the sensitivity of the sensor is increasing from 2.7 nm/RIU (refractive index unit) for pure water (with 1.3330 RIU) to 6.5 nm/RIU for pure IPA (with 1.3772 RIU). The increasing sensitivity of the sensor with increasing refractive index of the surrounding media is caused by the increasing evanescent field volume of the guided light, leaking out of the surface of the waveguide. Considerably, the sensitivity reaches its maximum, if the medium has a refractive index close to the refractive index of the waveguide (<1.58). In comparison with the uncoated eFBG sensor from Eisner et al., which possessed a central Bragg wavelength of 852 nm and achieved a sensitivity of 1.33 nm/RIU in 1.33–1.36 RIU, while in 1.4–1.43 RIU, the sensitivity increases to approximately 3.79 nm/RIU [23], our RWBG sensor demonstrates an increased sensitivity.

Furthermore, according to the response time of the RWBG sensor and considering the overall volume of the T-junction structure is about 7 mm^3, we are able to estimate the average volume flow rate of the aqueous solutions inside the microchannels to be 0,06 mm^3/s. Here we assume, that the sensor is responding instantaneously and hence the response time represents the time needed to cover the sensor completely with the injected fluid (until the wavelength shift reaches a stabilized position). In cases of more complicated LOC device structures for specific application, the local flow rate can depend on different structures in the LOC and may not be measured accurately from the external pump rate. Therefore, this experiment also demonstrates the potential of the RWBG sensor applied for in-situ flow rate monitoring.

3.3. Gas-phase Hydrogen Selective Measurement

For the selective gas-phase hydrogen detection, the RWBG sensor coated with palladium nanoparticles was enclosed in an experimental gas chamber that allows gas flow regulated with a multi-gas mass flow controller (see section 2.5). The total gas flow was kept constant with 100 standard cubic centimeters per minute (sccm) by a multi-gas mass flow controller for all gas mixtures

Preprints (www.preprints.org) | NOT PEER-REVIEWED | Posted: 19 December 2023 doi:10.20944/preprints202312.1340.v1

applied. During the measurement, the RWBG sensor chip was exposed to nitrogen gas mixed with different concentrations of hydrogen up to 4 vol%, the measurement results are displayed in Figure 6.

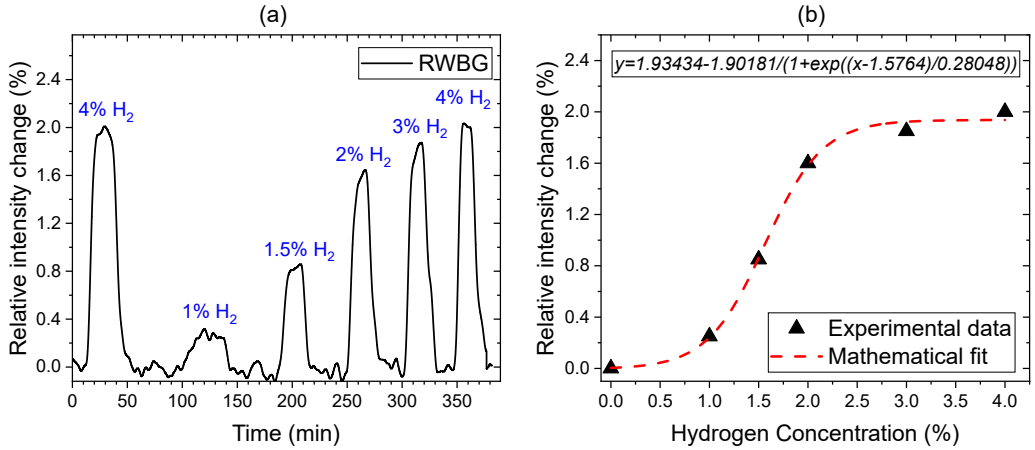

Figure 6. (**a**) Diagram displaying the time-resolved monitoring of the selective hydrogen gas measurement. (**b**) Plotted relative changes of the light intensity.

At the beginning of the measurement, the gas chamber is flushed with 100 vol% nitrogen for 15 min to ensure a pure environment for the sensing reaction. For each hydrogen measurement cycle, the sensor was exposed to hydrogen/nitrogen gas mixture, followed by a pure nitrogen gas flush. Figure 6(a) shows the monitored intensity change of the reflected Bragg grating signal regarding different hydrogen concentration in nitrogen. During the measurement, the light intensity of the SLED in the measurement setup (see Figure 3) shifted over time, therefore, the measurement results displayed in Figure 6(a) is corrected by a baseline to compensate for this effect. For each hydrogen level, a different and clear increase in signal intensity can be observed. The last flushing cycle using 4 vol% hydrogen concentration again demonstrates the reproducibility of measurement in comparison to the first cycle. The average response time for the signal intensity to reach a stabilized level lies at 120 s. For a more detailed analysis, the experimental results are plotted in Figure 6(b). The plotted measurement results reveal a non-linear signal intensity shift with increasing hydrogen concentration. Especially at hydrogen concentrations between 1-2 vol%, the sensitivity is higher. At 4 vol% hydrogen content, the sensor sensitivity decreases, but the signal intensity shift remains noticeable. For higher hydrogen concentrations above 5 vol%, the sensor response is saturated and is unable to show higher intensity shift. The overall intensity changes can be fitted using a nonlinear mathematical function. A similar non-linear sensitivity characteristic was also reported from other works, we assume that it is caused by the $\alpha - \beta$ phase transition of the palladium nanoparticles [18,24]. Despite the non-linear response, the RWBG sensor can still be used as hydrogen indicator.

4. Conclusion and outlook

In this manuscript, we demonstrated a multifunctional RWBG sensor integrated in a LOC device that can measure refractive indices of different concentrated aqueous solutions as well as temperatures. During the measurements, the RWBG sensor achieved a temperature sensitivity of -47.75 pm/K in an increasing temperature from 20 °C to 60 °C as well as a refractive index sensitivity of 6.5 nm/RIU from air to 99.9% pure IPA. When coated with palladium nanoparticles, the sensor achieved a reproducible hydrogen detection up to 4 vol%.

According to the presented measurements, our RWBG sensor shows a promising potential for applications based on LOC concept. The demonstrated sensing performance for temperature, refractive index and selective gas measurements can be used in various LOC-based chemical applications like in-situ sensing of temperature or concentration of the liquid solutions in the microchannel. Additionally, with the palladium nanoparticle functional coating, the RWBG sensor chip can be

applied for applications like investigating the underground bio-methanation concept, indicating the remaining hydrogen level during the methanation process.

For future works, the RWBG sensor could be further optimized to pursue higher sensing accuracy and open more potentials. For example, the polymer ridge waveguide can be inscribed with multiple Bragg grating structures in different wavelength areas at different positions, forming a sensor multiplexing array. In this case, different sensors could provide referencing data that compensates disruptive effects like undesired temperature influences, resulting in an increased sensor accuracy.

Funding: This research was funded by German Federal Ministry for Economy (BMWi) under grant agreement No. ZF4058510JA9 (ZIM-fluidSens).

Data Availability Statement: Data will be made available on request.

Acknowledgments: The authors would like to thank HOT microfluidics GmbH for the cooperation within the research project ZIM-fluidSens.

Conflicts of Interest: The authors declare no conflict of interest.

References

1. Dittrich, P.S.; Manz, A. Lab-on-a-chip: microfluidics in drug discovery. *Nature Reviews Drug Discovery* **2006**, *5*, 210–218.
2. Ríos, Á.; Zougagh, M.; Avila, M. Miniaturization through lab-on-a-chip: Utopia or reality for routine laboratories? A review. *Analytica Chimica Acta* **2012**, *740*, 1–11.
3. Azizipour, N.; Avazpour, R.; Rosenzweig, D.H.; Sawan, M.; Ajji, A. Evolution of Biochip Technology: A Review from Lab-on-a-Chip to Organ-on-a-Chip. *Micromachines* **2020**, *11*.
4. Hamid, I.A.; Kamil, Y.M.; Manaf, A.A.; Mahdi, M.A. Fabrication and characterization of micro fluidic based fiber optic refractive index sensor. *Sensing and Bio-Sensing Research* **2017**, *13*, 70–74.
5. Butt, M.A.; Kazanskiy, N.L.; Khonina, S.N. Advances in Waveguide Bragg Grating Structures, Platforms, and Applications: An Up-to-Date Appraisal. *Biosensors* **2022**, *12*.
6. Kashyap, R. *Fiber Bragg Gratings*; Academic Press, 2009.
7. Kawasaki, B.S.; Hill, K.O.; Johnson, D.C.; Fujii, Y. Narrow-band Bragg reflectors in optical fibers. *Optics Letters* **1978**, *3*, 66–68.
8. Rao, Y. Recent progress in applications of in-fibre Bragg grating sensors. *Optics and Lasers in Engineering* **1999**, *31*, 297–324.
9. Liang, W.; Huang, Y.; Xu, Y.; Lee, R.K.; Yariv, A. Highly sensitive fiber Bragg grating refractive index sensors. *Applied Physics Letters* **2005**, *86*.
10. Lee, S.M.; Jeong, M.Y.; Saini, S.S. Etched-Core Fiber Bragg Grating Sensors Integrated With Microfluidic Channels. *Journal of Lightwave Technology* **2012**, *30*, 1025–1031.
11. Dong, L.; Cruz, J.L.; Reekie, L.; Archambault, L. Tuning and chirping fiber Bragg gratings by deep etching. *IEEE Photonics Technology Letters* **1995**, *7*, 1433–1435.
12. Meyer, J.; Nedjalkov, A.; Kelb, C.; Strobel, G.J.; Ganzer, L.; Schade, W. Manufacturing and Characterization of Femtosecond Laser-Inscribed Bragg Grating in Polymer Waveguide Operation in an IR-A Wavelength Range. *Sensors* **2020**, *20*, 249.
13. Kumar N, V.; BS, K.; Asokan, S. Selective detection of lead in water using etched fiber Bragg grating sensor. *Sensors and Actuators B: Chemical* **2022**, *354*.
14. S, S.; Vasu, K.S.; Bhat, N.; Asokan, S.; Sood, A.K. Ultra sensitive NO2 gas detection using the reduced graphene oxide coated etched fiber Bragg gratings. *Sensors and Actuators B: Chemical* **2016**, *223*, 481–486.
15. Kefer, S.; Dai, J.; Yang, M.; Schmauss, B.; Hellmann, R. Hypersensitive H2 sensor based on polymer planar Bragg gratings coated with Pt-loaded WO3-SiO2. *Optics Letters* **2020**, *45*, 3601–3604.
16. Strobel, G.J.; Hagemann, B.; Huppertz, T.M.; Ganzer, L. Underground bio-methanation: Concept and potential. *Renewable and Sustainable Energy Reviews* **2020**, *123*, 109747.
17. Farajzadeh, R.; Bartholomeus, P.L.; Hajibeygi, H.; Bruining, J. Exergy Return on Exergy Investment and CO2 Intensity of the Underground Biomethanation Process. *ACS Sustainable Chemistry & Engineering* **2022**, *10*, 10318–10326.

18. Abdalwareth, A.; Flachenecker, G.; Angelmahr, M.; Schade, W. Optical fiber evanescent hydrogen sensor based on palladium nanoparticles coated Bragg gratings. *Sensors and Actuators A: Physical* **2023**, *361*.
19. Micro Resist Technology GmbH. Technical sheet EpoCore and EpoClad.
20. Burgmeier, J.; Waltermann, C.; Flachenecker, G.; Schade, W. Point-by-point inscription of phase-shifted fiber Bragg gratings with electro-optic amplitude modulated femtosecond laser pulses. *Optics Letters* **2014**, *39*, 540–543.
21. Pospori, A.; Ioannou, A.; Kalli, K. Temperature and Humidity Sensitivity of Polymer Optical Fibre Sensors Tuned by Pre-Strain. *Sensors* **2022**, *22*.
22. Chu, K.Y.; Thompson, A.R. Densities and Refractive Indices of Alcohol-Water Solutions of n-Propyl, Isopropyl, and Methyl Alcohols. *Journal of Chemical and Engineering Data* **1962**, *7*, 358–360.
23. Eisner, L.; Flachenecker, G.; Schade, W. Doped silica sol layer coatings on evanescent field fiber Bragg gratings for optical detection of nitroaromate based explosives. *Sensors and Actuators A: Physical* **2022**, *343*.
24. Schroeder, K.; Ecke, W.; Willsch, R. Optical fiber Bragg grating hydrogen sensor based on evanescent-field interaction with palladium thin-film transducer. *Optics and Lasers in Engineering* **2009**, *47*, 1018–1022.